

High-speed liquid lens with 2-ms response and 80.3-nm root-mean-square wavefront error

Hiromasa Oku^a and Masatoshi Ishikawa^a

^aGraduate School of Information Science and Technology, The University of Tokyo, 7-3-1 Hongo, Bunkyo-ku, Tokyo, Japan

ABSTRACT

A liquid lens structure with a step response time of 2 ms, a refractive power range of 52 D, and a root-mean-square (RMS) wavefront error of 80.3 nm is reported. This lens uses a liquid–liquid interface with a pinned contact line as a variable refractive surface, and its shape is controlled by a piezo stack actuator via a built-in hydraulic amplifier. The potential applications of this device include axial focus scanning of microscopes and focusing/zooming of camera lenses and machine vision systems.

Keywords: liquid lens, variable focus, high speed, millisecond, Dynamorph Lens

1. INTRODUCTION

Recently, digital vision systems such as digital cameras, hand-held video cameras, and computer vision systems have been getting popular. Such vision systems are typically composed of imaging optics, a digital imager, and a processor. Among these three components, two of them, the imager and processor, have been showing rapid performance improvements, particularly the response speed. Recent studies have reported a vision system that can acquire and process one image in 1 ms.^{1–3} Meanwhile, the other component, the imaging optics, has a much slower response time, generally from 0.1 to 1 s for focusing or zooming. This is because, in most consumer imaging optics, one or more lenses must be moved, which takes considerable time due to the lens mass. As a result, dynamic control of the optics tends to be a speed bottleneck of the whole vision system. For this reason, most vision systems avoid dynamic control of the optics when they need fast response speed. If a suitable high-speed focusing device could be realized, the response time for focusing or zooming could be shortened, and the above problem could be completely eliminated. In addition, such devices have long been sought in a wide range of fields, such as consumer imaging optics, microscopy, endoscopy, and computer vision.

Our goal is to develop a variable-focus lens with a response time of 1 ms and a peak-to-valley (P-V) wavefront error (WFE) of $\lambda/4$, where λ is wavelength. The target response time was set by considering that high-speed image processing systems capable of processing each frame in less than 1 ms have already been realized. The target WFE was set based on the well-known Rayleigh criterion of a quarter-wave optical path difference that is regarded as a standard of image quality.⁴

Many studies have reported various types of variable-focus lenses, for example, those based on the electro-optic effect,⁵ liquid crystals,^{6–11} and deformation of a refractive surface.^{12–14} Production of practical focusing devices with both high response speed and high optical performance is, however, still a challenge. A liquid interface is known to be suitable for the surface of such a lens due to its almost perfect spherical shape and deformability.^{15–22} Therefore, liquid lenses show great potential to realize both high-speed focusing and high optical performance.^{23–25} Moran et al. reported a liquid–air interface driven by liquid pressure and demonstrated 20-ms response time.²⁴ López et al. reported a liquid lens using a liquid–air interface driven by lens oscillation and demonstrated harmonic oscillation of focusing at 100 Hz.²⁵ However, their response time is longer than 1 ms, and in addition, their mechanism cannot eliminate the effect of gravity due to the use of a liquid–air interface. Thus, it is difficult to achieve high resolution. To the best of our knowledge, there have been no previous studies that have achieved our goals stated above.

Further author information: (Send correspondence to H.O.)

H.O.: E-mail: Hiromasa.Oku@ipc.i.u-tokyo.ac.jp, Telephone: +81-3-5841-6937

M.I.: E-mail: Masatoshi.Ishikawa@ipc.i.u-tokyo.ac.jp, Telephone: +81-3-5841-8602

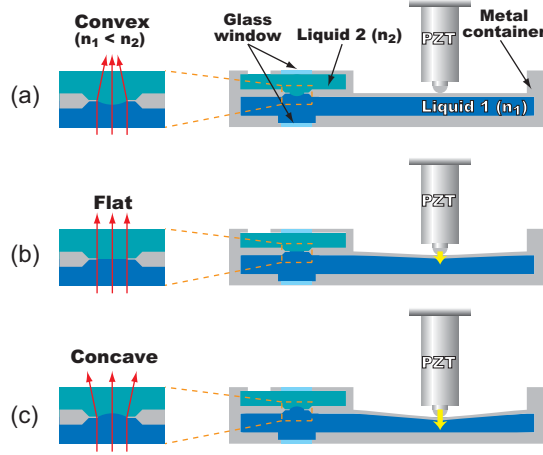


Figure 1. Cross-sectional views of the developed lens structure to illustrate its focusing mechanism.²⁶ The interface shown at the left works as a deformable refractive surface. Two liquids with refractive indexes of n_1 and n_2 are interfaced at the circular aperture shown at the left. Light rays are drawn assuming $n_1 < n_2$.

In this article, we report a liquid lens using a liquid–liquid interface that can arbitrarily control the focal length in milliseconds and achieve practical imaging performance. The lens is called a *dynamorph lens (DML)* since it deforms its interface dynamically. Although an overview of this lens has already been reported,²⁶ we report details of the lens in this article.

2. DYNAMORPH LENS

In a previous study, a variable-focus lens with 1-kHz bandwidth using the deformation of a thin glass plate was reported.¹³ Although the response time of the lens was fast, its resolution was low due to the radial profile of the deformable surface. The radial deformation of a circular plate is theoretically described by a 4-th order polynomial.¹³ A lens with this radial profile includes large spherical aberration that is difficult to be corrected. To solve this problem, our idea was to replace the glass plate with a liquid–liquid interface, which is known to have a good spherical profile, so that the structure could achieve both high-speed response and high-resolution.

2.1 Focusing Mechanism

Fig. 1 schematically shows the cross-section of the proposed lens. This lens dynamically changes the curvature of the interface by means of liquid pressure. Two immiscible liquids, indicated as liquids 1 and 2, are infused in two chambers, but they are interfaced at a circular hole that works as an aperture of the lens. This interface acts as a refractive surface having optical power due to the different refractive indexes of the two liquids. One chamber (the lower chamber in Fig. 1) is equipped with a deformable wall that a piezo stack actuator thrusts to change the chamber volume. When the piezo stack actuator extends, the lower chamber volume decreases, and the surplus liquid volume presses the interface to change its shape from convex to concave. Since the actuator deforms the wall quickly, the dimensions of the deformable wall should be designed to have a high natural frequency of about 10 kHz,¹³ otherwise undesired vibrations would be excited.

Although the displacement of the piezo stack actuator can be controlled at a frequency on the order of kilohertz, its stroke is quite short, about 10 μm . Since this is too short to achieve a sufficient range of refractive power, a built-in motion amplifier¹³ is used. The area of the deformable wall pressed by the piezo stack actuator (S) is much larger than that of the lens surface (s), so that the change in the lens surface shape is approximately S/s times that of the deformable wall.

When the lens aperture is several millimeters, the required volume to change the interface curvature is on the order of microliters ($= \text{mm}^3$). A flow channel for liquid 1 is designed to have a cross-sectional area of several tens of mm^2 so that the flow speed is sufficiently small. This is because viscosity resistance tends to increase with faster flow speed, and large resistance should be avoided to achieve high-speed response.

2.2 Forming Spherical Liquid–Liquid Interface

The liquid–liquid interface must be able to morph dynamically and readily and also to form a good spherical meniscus, in order to achieve high response speed and good resolving power.

To achieve high response speed, the aperture structure was designed to be able to fix the contact line, which is an intersection between the interface and the aperture wall. A circular edge structure is formed in the aperture to pin the contact line like the rim of a cup filled to the brim with water. An interface with a pinned contact line tends to have a higher natural frequency than that of an interface with a free contact line;²⁷ i.e., the contact line can move freely along the wall. Thus, an interface with a pinned contact line is suitable for achieving high-speed response.

A previous study of a liquid lens driven based on the electro-wetting phenomenon¹⁸ reported underdamped, critically damped, and overdamped responses of a meniscus, like a damped mass–spring system. Although the contact line was free in that study due to the driving mechanism, similar behavior was also observed with our structure using a pinned contact line. For high-speed response, a critically damped response is suitable because the shortest response time can be achieved.

Forming a good spherical meniscus is essential to achieve high resolving power. A liquid–liquid interface has surface energy that is proportional to the area with a proportionality coefficient of surface tension. When the liquid volume is constant, the interface tends to form a spherical shape to reduce its area, which is an ideal feature that can be exploited for use as the refractive surface of a lens. In the case of a meniscus, the interface also forms a partially spherical shape if its contact line is ideally circular. An actual meniscus, however, includes deformation caused by contact line deformation and the effects of external forces, including gravity. These effects should be eliminated to form a good spherical meniscus. Though our goal is to form a spherical surface, note that a spherical shape is not always the best shape for a lens device, and there is a possibility of using these effects to form an aspherical interface to achieve better optical performance.

The pinned contact line should be a well-formed circle in three dimensions to realize a good spherical meniscus. According to a study on a slightly deformed axisymmetric liquid drop,²⁸ distortions of the interface due to deformation of the contact line exist up to the center of the unperturbed meniscus. Such distortions, however, reduce with distance from the contact line. Assuming that this result is also true for the interface of our lens, the largest deformation of the interface could be limited by the largest contact line deformation. As a tolerance of the contact line deformation, one-quarter of the wavelength is adopted considering the Rayleigh quarter-wave criterion.²⁹ The criterion itself is the tolerance of wavefront error, and not of the deformation from a spherical shape. Thus, the tolerance has no direct relevance to optical performance. However, we considered the quarter-wavelength as an optically small deformation and adopted it as the tolerance for convenience sake.

When there is a difference between the densities of two liquids, the meniscus is deformed by gravity. The effect of gravity can be roughly estimated from the capillary length, l_c . The capillary length is a characteristic length scale for a fluid subject to gravity and surface tension. When the scale of the fluid is shorter than the capillary length, surface tension is the dominant force, and the effect of gravity is small. In contrast, when the scale of the fluid is longer than the capillary length, gravity is the dominant force. The capillary length of the liquid interface is denoted as:

$$l_c = \sqrt{\frac{\sigma}{|\rho_1 - \rho_2|g}} \quad (1)$$

where σ is surface tension, ρ_1 and ρ_2 are the liquid densities, and g is the gravitational constant. When the lens aperture diameter d is sufficiently smaller than the capillary length ($d < l_c$), gravity is negligible.

3. EXPERIMENTS

3.1 Prototype

A prototype of the Dynamorph Lens was developed based on the above structure. Its photograph is shown in Fig. 2 (a). The aperture’s diameter was 3.0 mm, and that of the deformable wall was 24.0 mm.

Ultra pure water (refractive index $n_1 = 1.33$) purified by DirectQ-UV (Millipore) and poly-dimethyl-siloxane (PDMS) were used as the immiscible liquids. PDMS is a kind of silicon-based organic polymer, and it is an

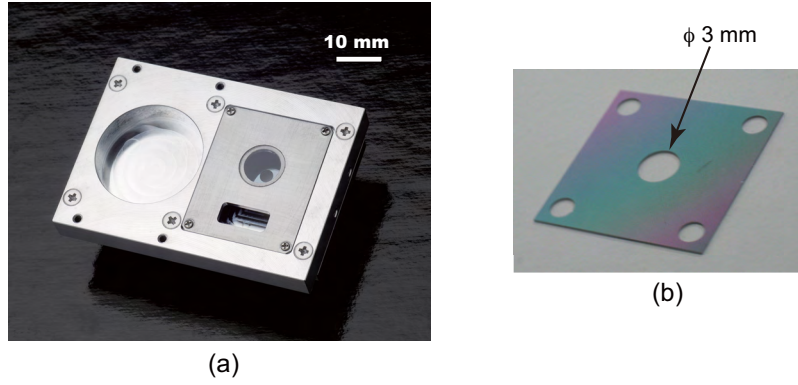


Figure 2. Photographs of the developed prototype (a) and its aperture part (b). Circular hole shown at the right side of (a) is an aperture. The bottom of the hollow at the left side of (a) is a circular deformable wall. The piezo stack actuator (PZT) pushes the center of the wall. The center hole of the aperture part works as a lens aperture (b). The other four through-holes are for screws.

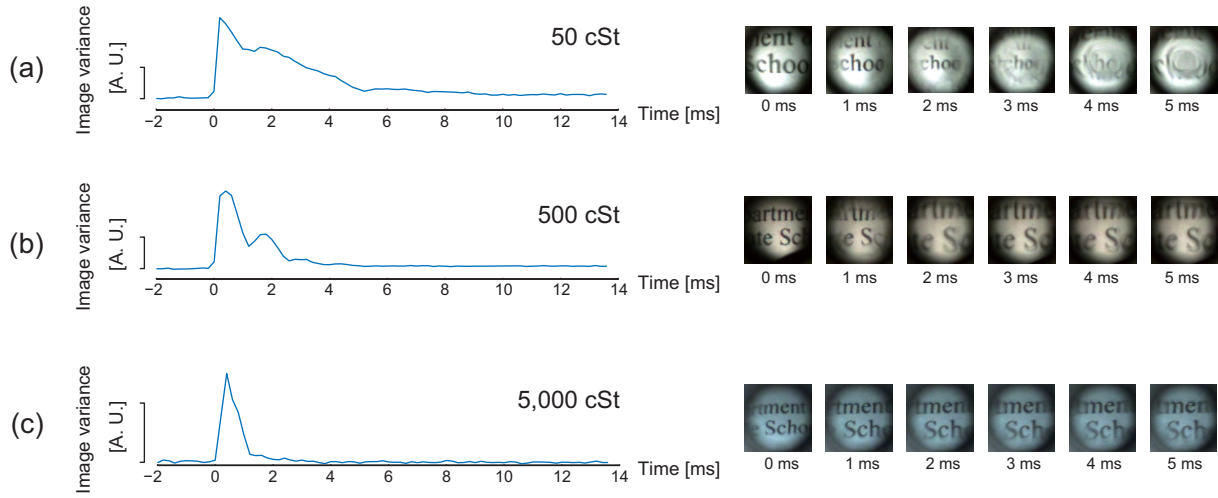


Figure 3. Three kinds of transient responses observed for infused PDMSs with kinematic viscosities of (a) 50 cSt, (b) 500 cSt, and (c) 5000 cSt.²⁶ Profiles of image variance $\sum_x \sum_y |I(x, y; t) - I(x, y; t - 1)|$ and captured image sequences are shown, where $I(x, y; t)$ is the intensity of the pixel at (x, y) in the t -th frame.

optically transparent liquid. Its kinematic viscosity depends on the number of repeating monomers, and PDMSs with a wide range of kinematic viscosities (from 10 to 10^5 centistokes (cSt)) are commercially available. This means that the relationship between the dynamic behavior of the interface and the liquid's viscosity could be studied easily.

As a preliminary measurement of its transient response depending on the PDMS's viscosity, images obtained through the interface during its transient response were captured using a high-speed camera with a frame rate of 5000 fps.²³ These results were obtained using the previous prototype, whose aperture structure was different from the structure described above. Three kinds of PDMSs with different kinematic viscosities of 50, 500 and 5000 cSt (KF-96- $\{50, 500, 5000\}$ cs, Shin-Etsu Silicones) were used, together with ultra-pure water. An overdamped response was obtained with the 5000 cSt PDMS (Fig. 3 (c)), and image distortion was observed with the 50 and 500 cSt PDMSs (Fig. 3 (a) and (b), respectively). The 5000 cSt PDMS (refractive index $n_2 = 1.40$) was used for further experiments, described below. It should be possible to achieve a critically damped response with an intermediate kinematic viscosity between 500 cSt and 5000 cSt. However, more detailed evaluation of the dynamic behavior is now under study and will be reported later.

Ultra-pure water was infused in the chamber having the deformable plate to transmit the pressure generated by the actuator. If the viscosity of water is not negligible, the pressure transmission would take much time and the response speed would be slow. The effect of viscosity can be roughly estimated using the boundary layer approximation,³⁰ which assumes that the viscous forces are negligible except within a thin layer close to the solid boundaries. The thickness of the boundary layer δ is on the order of $\sqrt{\nu t}$ where ν is the kinematic viscosity, and t is time originating at the beginning of flow. Assuming a step-like pressure input, and taking the kinematic viscosity of water to be about $1 \text{ cSt} = 10^{-6} \text{ m}^2/\text{s}$, the boundary layer thickness of water, δ_W , 1 ms after the pressure input is

$$\delta_W \sim 3 \times 10^{-5} = 30 \mu\text{m}$$

. Since the developed prototype has millimeter-sized chambers, which is much larger than the boundary layer thickness, the viscous resistance of water can be neglected. In the same manner, the boundary layer thickness of the 5000 cSt PDMS can be also estimated as $\delta_{\text{PDMS}} \sim 2 \text{ mm}$. This is of the same order as the lens aperture, and therefore, the viscous resistance of the PDMS cannot be neglected. This is consistent with the overdamped response of the interface.

In the prototype, the acceptable vertical deformation, Δ , of the contact line parallel to the optical axis is $\Delta < (1/4)\lambda/(n_2 - n_1)$, where λ is wavelength. Assuming $\lambda = 546 \text{ nm}$ and $\Delta < 1.95 \mu\text{m}$, a machining accuracy of less than $1.95 \mu\text{m}$ is required for the circular edge pinning the contact line. To achieve this accuracy, the edge of the aperture was made from a silicon substrate with a hole formed in it by photolithography to achieve the required accuracy. A photograph is shown in Fig. 2 (b).

The capillary length, l_c , of the prototype was 12.7 mm, using the density difference between water (0.997 g/cm^3) and PDMS (0.975 g/cm^3) of 22 kg/m^3 , an interface tension between water and PDMS of 34.8 mN/m was measured by the pendant drop method, and acceleration of gravity was assumed to be 9.8 m/s^2 . Since the lens aperture diameter of 3 mm is much smaller than the capillary length, the effect of gravity should be quite small.

The interface behavior seemed very sensitive to contamination on the walls. Thus, before infusing the liquids, every part of the prototype was ultrasonically cleaned using water containing detergent, rinsed with ultra-pure water, and desiccated in a clean-bench. If this was not done, the meniscus tended to be deformed and its optical performance was reduced.

3.2 Optical Properties

Wavefront errors (WFE) of the prototype were measured with a Shack-Hartmann wavefront sensor (OMI, SpotOptics) equipped with a metal halide lamp (Sigma Koki). During the measurement, the prototype was placed vertically with the aperture plane parallel to the direction of gravity; that is, the interface deformation due to gravity was maximum. The actuator was not operated in order to fix the focal length. The focal length was adjusted by moving the actuator position using a manual translation stage. When the focal length was positive, parallel light collimated by the prototype from a pinhole ($\phi 100 \mu\text{m}$ or $\phi 200 \mu\text{m}$ depending on the focal length) provided by the manufacturer was input to the sensor. The S-H sensor needs a reference wavefront. A collimated light wavefront from a collimator provided by the manufacturer was captured as a reference. When the focal length was infinity and the interface was flat, parallel light passing through the prototype from the collimator was input to the sensor. A collimated light wavefront was also used as a reference. When the focal length was negative, a collimated light wavefront produced by a macro lens (Edmund Optics) from the pinhole ($\phi 100 \mu\text{m}$) was captured as a reference. Then, the prototype was inserted between the pinhole and the macro lens. The position of the pinhole was adjusted so that the exit light from the macro lens was collimated. The collimated light wavefront originating from the reference was measured as the WFE. The focal length of the prototype was estimated from the positional relationship of the pinhole and the prototype (positive focal length), or the pinhole, the prototype, and the macro lens (negative focal length).

Nine WFEs with different focal lengths ranging from -44 mm to $-\infty$ and ∞ to 42 mm were measured. Fig. 4 shows the WFE profiles, from which tilt and defocus components are subtracted, together with peak-to-valley (PV) WFE and root-mean-square (rms) WFE values for each focal length. The XY plane is at the exit pupil of the prototype, and the Z axis shows the WFE at each location in the pupil. Since the pupil is circular, the

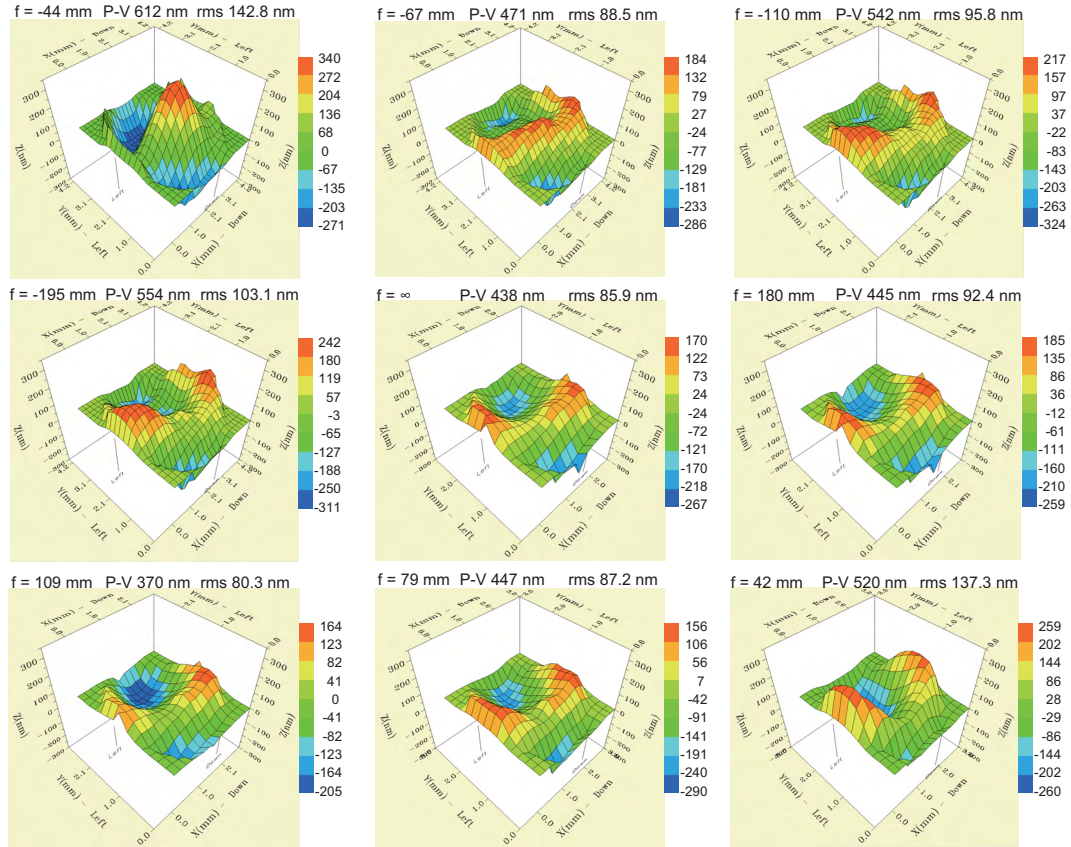


Figure 4. Nine wavefront error (WFE) profiles with different focal lengths.

WFE values outside of the pupil are plotted as zero. The minimum WFEs of 370 nm (P-V) and 80.3 nm (rms) were achieved with the focal length of 109 mm. The maximum WFEs of 612 nm (P-V) and 142.8 nm (rms) were achieved with the focal length of -44 mm. The WFE tends to be worse when the curvature of the interface is small and the absolute refractive power is high. From the wavefront profiles, the WFEs on the contact line seem to be around 300–600 nm (P-V). These WFEs correspond to $\lambda/2$ – λ , equivalent to a vertical deformation of the contact line of about 4–8 μm , assuming that the WFE occurred due to deformation of the interface. These deformations are much larger than our target of 1.95 μm described above. Although the cause of this discrepancy is now under study, deformation of the aperture structure or failure to form the contact line at the proper place are potential causes. Note that the peak and valley of the wavefront were almost always on the contact line, except for the cases of $f = -44$ mm and $f = 42$ mm. Thus, the assumption that the meniscus deformation should be limited by that of the contact line seems valid when the meniscus curvature is small.

Nevertheless, the prototype achieved sufficient imaging performance for practical use. Fig. 5 shows a photograph of a USAF 1951 chart captured by a CMOS imager through the prototype with $f = 80$ mm and an object-side numerical aperture of 0.045. The 71.84 lp/mm bar chart was resolved by the lens.

Figure 6 shows how the refractive power depended on the displacement of the piezo stack actuator. A feedback-controlled piezo stack actuator system (custom-order, Mess-Tek) with a stroke of 20 μm and a minimum step response time of 1 ms was employed. The desired position of the actuator could be input as an analogue voltage, and its displacement, measured by a built-in capacitive sensor, could be monitored as an analogue voltage. The refractive power was estimated from the measured positions of an object, the prototype, and the projected image plane. A wide refractive power change of about 52 D was achieved with a displacement of only 12 μm . Note that the initial refractive power could be adjusted by altering the infused volume of water.

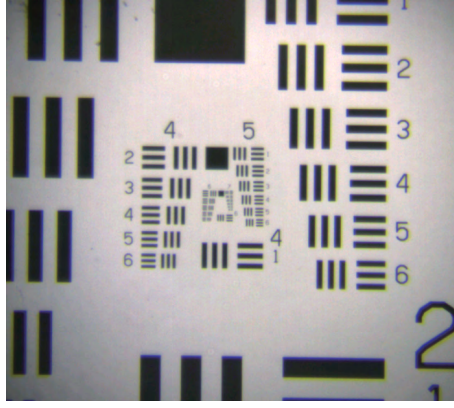


Figure 5. An image of USAF 1951 chart projected by the prototype with $f = 80$ mm.

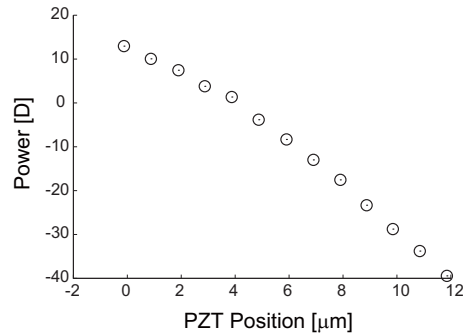


Figure 6. Refractive power plotted against the displacement of the piezo stack actuator.²⁶

3.3 Dynamic Response

A variable-focus macro lens system was developed using the prototype to demonstrate its fast focusing ability. Fig. 7 shows the system configuration. The position of the object plane could be shifted by changing the refractive power of the prototype. The prototype was driven by the same piezo stack actuator system described above. A projected image was captured by a high-speed camera (FASTCAM MC2.1, Photron) with 512x512 pixels at a frame rate of 2000 fps. This camera can start/stop recording in response to an external trigger signal. It can also output a digital signal for monitoring the exposure timing. A data logger (SL1000, Yokogawa) was used to record the instructions for and the actual positions of the actuator, the exposure signal of the high-speed camera, and the trigger signal described below.

All devices were synchronized using a trigger signal generated by a function generator (AFG320, Tektronix). It also generated a square wave as a desired position signal for the actuator. The high-speed camera and the data logger were set to start recording a given number of frames or samples in response to the trigger signal. While switching the actuator position, i.e., the focal length of the prototype DML, an operator manually operated the function generator to generate the trigger signal. Since the exposure timing of the high-speed camera was also recorded as a signal by the data logger, the exact exposure timing of each frame could be determined.



Figure 7. Variable-focus macro lens system using the prototype. O: object, DML: prototype Dynamorph Lens, L1: static lens relating exit pupil of DML to entrance pupil of macro lens. ML: conventional macro lens, HC: imager of high-speed camera.

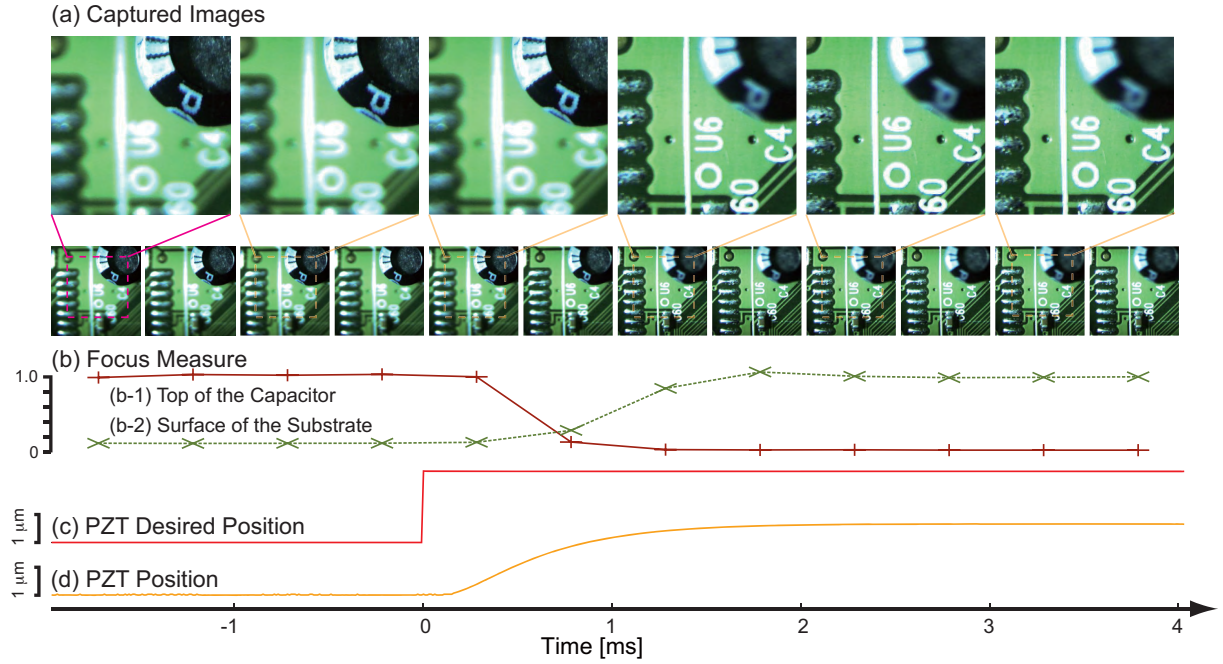


Figure 8. Step response of the prototype. Top image sequences were captured at 2000 fps through the prototype (a). The lower row shows a sequence of original captured images. The position of the left boundary of each image shows the starting time of its exposure. The upper row shows magnified images. Focus measures of two regions, the top of the capacitor and the substrate, were extracted from the captured images (b). They were normalized by the initial value (b-1) and the final value (b-2), respectively. The voltage input to the actuator (c) and the resulting position (d) are shown below.

The response time of the prototype was measured to be about 2 ms by capturing high-speed video through the prototype while switching its focal length every 10 ms. As a desired position signal, a square wave with a peak-to-peak amplitude of $2.5 \mu\text{m}$ and a frequency of 50 Hz was input to the piezo stack actuator. The response speed of the piezo stack actuator was adjusted so that clear images without distortion could be captured. Distorted images that seemed to be due to the underdamped response of the meniscus were observed when the response time of the actuator was set to be shorter, for example 1 ms. Fig. 8 (a) shows the captured image sequence from $t = -2$ to 4 ms as a step response. The focus was initially at the top of the capacitor ($t < 0$). A focus switch instruction was input to the piezo stack actuator at $t = 0$ (c). The image sequence shows that the focus position reached the substrate by $t = 2$ ms. As a measure of focus, the sum of horizontal and vertical Brenner gradients,³¹ $B = \sum_i^N \sum_j^M ([I(i, j) - I(i + m, J)]^2 + [I(i, j) - I(i, J + m)]^2)$ with $m = 2$, was adopted. Here, B is a numerical index of the amount of detail included in a digital image. A large B means that the area of the summations included in the calculation of B is in focus. To show the focus shift quantitatively, two focus measures were calculated for two different areas of the captured image: the top of the capacitor and the substrate. The profile of the focus measures also showed the 1.5 ms response of the focus switching (d). The distance from the substrate to the top of the capacitor was 12.1 mm.

When the actuator extends in length, it presses the deformable wall and generates positive pressure to morph the interface. The results shown in Fig. 8 were observed under this condition. In contrast, when the actuator shortens in length, the elastic force of the deformed wall generates negative pressure, morphing the interface in the reverse direction. Thus, the driving mechanism is different depending on the focusing direction. Fig. 9 shows step response results when the actuator shortened in length. Even in this case, the response time was about 2.5 ms, almost the same as the previous one.

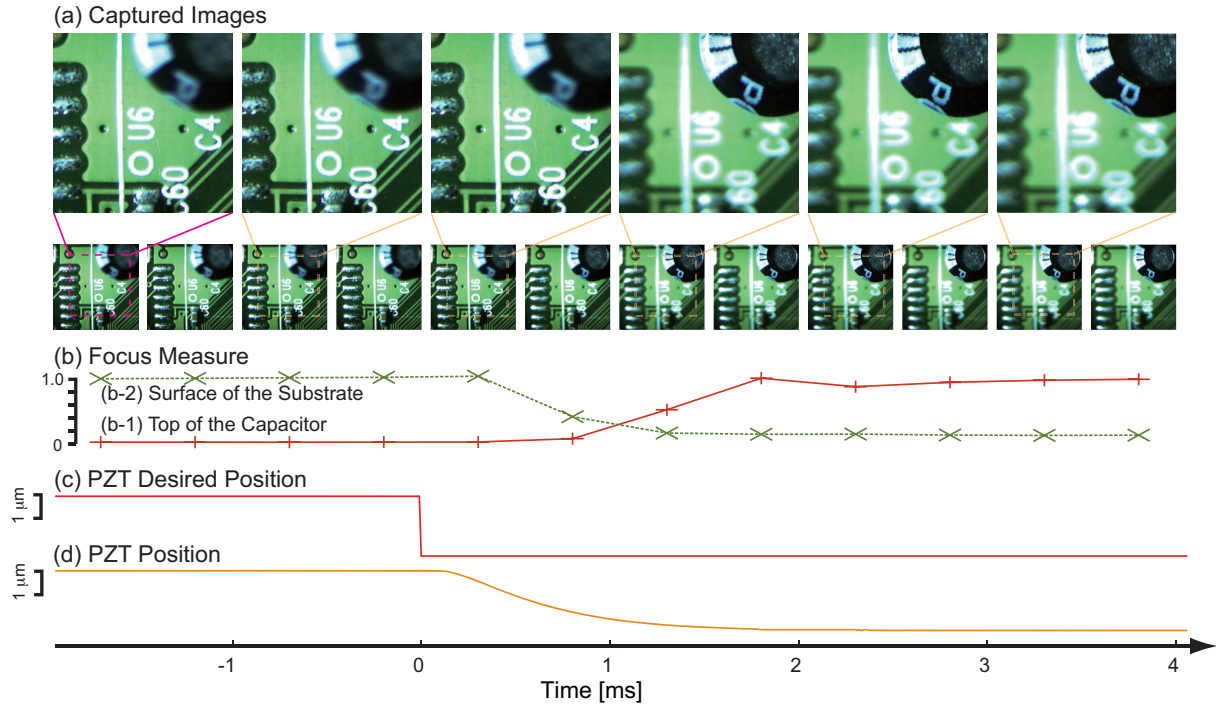


Figure 9. Reverse step response of the prototype.

4. DISCUSSION

The WFE of the current prototype is not sufficiently low considering the Rayleigh criterion, and the measured WFE shape suggested that the contact line was deformed, as described above. Assuming that contact line deformation was the cause, the WFE could be reduced by improving the mechanical parts to fix the contact line with higher precision.

Since the reported mechanism depends on the volume of liquid, and the liquid volume expands with an increase in temperature, when the temperature is more than 4 degrees Celsius in the case of water, the focal length drifts with the temperature change. This phenomenon was confirmed with our prototype. This could be solved by implementing feedback control of the device temperature using thermoelectric coolers such as Peltier elements, or by developing a special structure composed of a liquid and solid with negative thermal expansion coefficients that cancel the total volume expansion. Since all experiments were conducted on an optical bench whose heat capacity was quite large, the temperature of optical parts included in the prototype was kept constant during the experiments.

5. CONCLUSION

In this article, we reported a liquid lens using a liquid–liquid interface that can arbitrarily control the focal length in milliseconds and achieve practical imaging performance. The lens is called a *dynamorph lens (DML)* since it deforms its interface dynamically. A meniscus formed by a liquid–liquid interface with a pinned contact line was used as a refractive surface, and its curvature was controlled by a piezo stack actuator. Interface behavior similar to that of a damped mass–spring system was explained, and preliminary results obtained with a prototype were shown. Formation of a good spherical meniscus was discussed from the viewpoints of contact line deformation and the effect of gravity. Based on these discussions, a prototype was developed. A minimum rms WFE of 80.3 nm, a refractive power range of 52 D, and a step response time of 2 ms were demonstrated.

A fast focusing mechanism has long been sought in a wide range of fields, such as computer vision, microscopy, and endoscopy, and these fields are potential applications of our lens device reported here. Considering the con-

tinuous improvement of image processing systems, high-speed focusing mechanisms will become more important in the near future, and our lens is a promising candidate.

ACKNOWLEDGMENTS

The authors thank T. Hasegawa for his assistance in the experiments. This study was supported under the 2007 Industrial Technology Research Grant Program of the New Energy and Industrial Technology Development Organization (NEDO) of Japan.

REFERENCES

- [1] Komuro, T., Tabata, T., and Ishikawa, M., "A Reconfigurable Embedded System for 1000-fps Real-time Vision," *IEEE Transactions on Circuits and Systems for Video Technology*, to appear (2010).
- [2] Ishii, I., Kato, K., Kurozumi, S., Nagai, H., Numata, A., and Tamura, K., "Development of a Mega-pixel and milli-second Vision System using Intelligent Pixel Selection," *2004 1st IEEE Technical Exhibition Based Conference on Robotics and Automation (TExCRA 2004)*, 9–10 (2004).
- [3] Shimizu, K. and Hirai, S., "CMOS+FPGA Vision System for Visual Feedback of Mechanical Systems," *Proceedings of the 2006 IEEE International Conference on Robotics and Automation*, 2060–2065 (2006).
- [4] Smith, W. J., [*Modern Optical Engineering*], McGraw-Hill, Inc. (2000) (third edition).
- [5] Shibaguchi, T. and Funato, H., "Lead-Lanthanum Zirconate-Titanate (PLZT) Electrooptic Variable Focal-Length Lens with Stripe Electrodes," *Japanese Journal of Applied Physics, Part 1* **31**(9B), 3196–3200 (1992).
- [6] Eschler, J., Dickmann, S., and Mlynski, D. A., "Fast Adaptive Lens Based On Deformed Helical Ferroelectric Liquid Crystal," *Ferroelectrics* **181**, 21–28 (1996).
- [7] Hain, M., Glöckner, R., Bhattacharya, S., Dias, D., Stankovic, S., and Tschudi, T., "Fast switching liquid crystal lenses for a dual focus digital versatile disc pickup," *Optics Communications* **188**, 291–299 (2001).
- [8] Ren, H. and Wu, S.-T., "Inhomogeneous nanoscale polymer-dispersed liquid crystals with gradient refractive index," *Applied Physics Letters* **81**(19), 3537–3539 (2002).
- [9] Ren, H., Fan, Y.-H., and Wu, S.-T., "Tunable Fresnel lens using nanoscale polymer-dispersed liquid crystals," *Applied Physics Letters* **83**(8), 1515–1517 (2003).
- [10] Ren, H., Fan, Y.-H., and Wu, S.-T., "Liquid-crystal microlens arrays using patterned polymer networks," *Optics Letters* **29**(14), 1608–1610 (2004).
- [11] Wang, B., Ye, M., and Sato, S., "Liquid crystal lens with stacked structure of liquid-crystal layers," *Optics Communications* **250**, 266–273 (2005).
- [12] Kaneko, T., Ohmi, T., Ohya, N., Kawahara, N., and Hattori, T., "A New, Compact and Quick-Response Dynamic Focusing Lens," *TRANSDUCERS'97* **1**, 63–66 (1997).
- [13] Oku, H., Hashimoto, K., and Ishikawa, M., "Variable-focus lens with 1-kHz bandwidth," *Optics Express* **12**(10), 2138–2149 (2004).
- [14] Campbell, K., Fainman, Y., and Groisman, A., "Pneumatically actuated adaptive lenses with millisecond response time," *Applied Physics Letters* **91**, 171111 (2007).
- [15] Gorman, C. B., Biebuyck, H. A., and Whitesides, G. M., "Control of the Shape of Liquid Lenses on a Modified Gold Surface Using an Applied Electrical Potential across a Self-Assembled Monolayer," *Langmuir* **11**, 2242–2246 (1995).
- [16] Berge, B. and Peseux, J., "Variable focal lens controlled by an external voltage: An application of electrowetting," *The European Physical Journal E* **3**, 159–163 (2000).
- [17] Krupenkin, T., Yang, S., and Mach, P., "Tunable liquid microlens," *Applied Physics Letters* **82**(3), 316–318 (2003).
- [18] Kuiper, S. and Hendriks, B. H. W., "Variable-focus liquid lens for miniature cameras," *Applied Physics Letters* **85**(7), 1128–1130 (2004).
- [19] Cheng, C.-C., Chang, C. A., and Yeh, J. A., "Variable focus dielectric liquid droplet lens," *Optics Express* **14**(9), 4101–4106 (2006).

- [20] Ren, H. and Wu, S.-T., “Tunable-focus liquid microlens array using dielectrophoretic effect,” *Optics Express* **16**(4), 2646–2652 (2008).
- [21] López, C. A., Lee, C.-C., and Hirs, A. H., “Electrochemically activated adaptive liquid lens,” *Applied Physics Letters* **87**, 134102 (2005).
- [22] Dong, L., Agarwal, A. K., Beebe, D. J., and Jiang, H., “Adaptive liquid microlenses activated by stimuli-responsive hydrogels,” *Nature* **442**, 551–554 (2006).
- [23] Oku, H. and Ishikawa, M., “Rapid Liquid Variable-Focus Lens with 2-ms Response,” *19th Annual Meeting of the IEEE Lasers & Electro-Optics Society (LEOS 2006)*, 947–948 (2006).
- [24] Moran, P. M., Dharmatilleke, S., Khaw, A. H., Tan, K. W., Chan, M. L., and Rodriguez, I., “Fluidic lenses with variable focal length,” *Applied Physics Letters* **88**, 041120 (2006).
- [25] López, C. A. and Hirs, A. H., “Fast focusing using a pinned-contact oscillating liquid lens,” *Nature Photonics* **2**, 610–613 (2008).
- [26] Oku, H. and Ishikawa, M., “High-speed liquid lens with 2 ms response and 80.3 nm root-mean-square wavefront error,” *Applied Physics Letters* **94**, 221108 (2009).
- [27] Miles, J., “The capillary boundary layer for standing waves,” *Journal of Fluid Mechanics* **222**, 197–205 (1991).
- [28] Shanahan, M. E. R., “Meniscus shape and contact angle of a slightly deformed axisymmetric drop,” *Journal of Physics D: Applied Physics* **22**, 1128–1135 (1989).
- [29] Fischer, R. E. and Tadic-Galeb, B., [*Optical System Design*], McGraw-Hill (2000).
- [30] Kundu, P. K. and Cohen, I. M., [*Fluid Mechanics*], Elsevier Academic Press (2004) (third edition).
- [31] Brenner, J. F., Dew, B. S., Horton, J. B., King, T., Neurath, P. W., and Selles, W. D., “An Automated Microscope For Cytologic Research. A Preliminary Evaluation,” *The Journal of Histochemistry and Cytochemistry* **24**(1), 100–111 (1976).